

MaskClustering: View Consensus based Mask Graph Clustering for Open-Vocabulary 3D Instance Segmentation

Mi Yan^{1,2} Jiazhao Zhang^{1,2} Yan Zhu¹ He Wang^{1,2,3}
¹Peking University, ²Beijing Academy of Artificial Intelligence ³Galbot

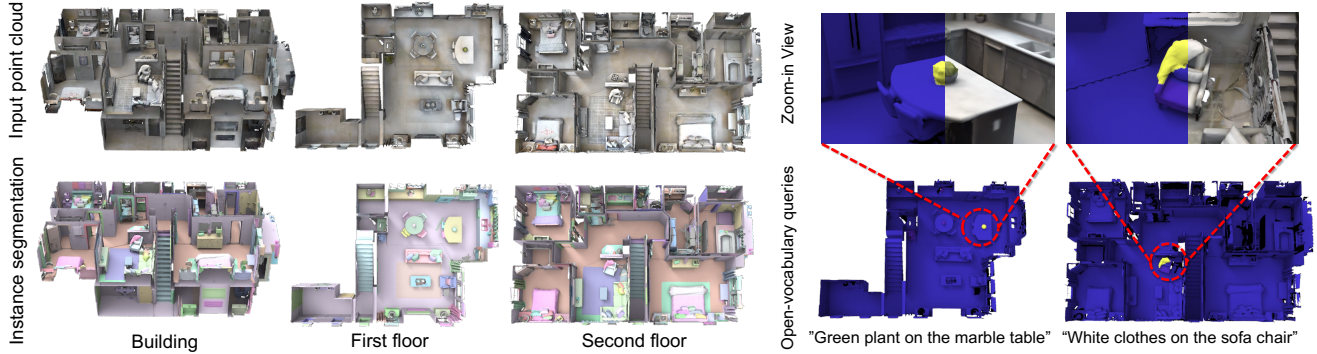


Figure 1. Our method tackles the challenges of open-vocabulary instance segmentation. It achieves detailed segmentation across objects of varying scales and can query these objects using free-form text.

Abstract

Open-vocabulary 3D instance segmentation has emerged as a frontier topic due to its capability to segment 3D instances beyond a predefined set of categories. However, compared to significant progress in the 2D domain, methods for 3D open-vocabulary instance segmentation are hindered by the limited scale of high-quality annotated 3D data. To harness the capabilities of 2D models, recent efforts have focused on merging 2D masks based on metrics such as geometric and semantic similarity to form 3D instances. In contrast to these local metrics, we propose a novel metric called view consensus to better exploit multi-view observation. The key insight is that two 2D masks should be considered as belonging to the same instance if a considerable number of other 2D masks from other views contain both these two masks. Based on this metric, we build a global mask graph and iteratively cluster masks, prioritizing mask pairs with solid view consensus. The corresponding 3D points cluster of these 2D mask clusters can be regarded as 3D instances, along with the fused open-vocabulary features from clustered 2D masks. Through this multi-view verification and fusion mechanism, our method effectively leverages the prior instance knowledge from massive 2D masks predicted by visual foundation models, eliminating the need for training on 3D data. Experiments on publicly available datasets, including ScanNet200 and MatterPort3D, demonstrate

that our method achieves state-of-the-art performance in both open-vocabulary instance segmentation and class-agnostic mask generation. Our project page is at <https://pku-epic.github.io/MaskClustering/>

1. Introduction

Open-vocabulary 3D instance segmentation tackles the problem of predicting 3D object instance masks and their corresponding categories from reconstructed 3D scene representations without relying on a predefined list of categories. This task plays a crucial role in advancing 3D scene understanding [4, 10, 33], robotics [7, 13, 45] and VR/AR applications [20, 42]. However, this task is more challenging than its established 2D counterpart, open-vocabulary 2D instance segmentation [9, 18, 36, 40, 41], primarily due to the lack of large-scale open-world 3D data. Consequently, most current methods [16, 27, 35] in this field divide this task into two stages: zero-shot 3D instance mask generation, followed by open-vocabulary semantic queries. In this work, we primarily focus on obtaining high-quality, zero-shot 3D instance masks.

Existing approaches for zero-shot 3D instance mask generation primarily follow two paths. A line of work is based on 2D-to-3D region grow-based methods [7, 27, 43] that processes frames sequentially and continuously updates a list of 3D instances. This method associates new 2D masks

with existing 3D instances based on geometric overlap and semantic similarity, subsequently fusing them. However, we observe that these online processing methods lack global optimality across all frames and often suffer from over-segmentation issues especially for large objects due to imperfect criteria in geometric overlap or semantic similarity. In contrast, 3D-to-2D projection-based methods [16, 17] leverage existing 3D instance segmentation algorithms to generate 3D masks. However, this approach is fundamentally constrained by the quality of 3D reconstructions and the relatively modest capabilities of current 3D instance segmentation tools. As a result, these methods often struggle to accurately segment small and detailed objects, leading to a significant loss of detail and precision in complex scenes.

To address these limitations, we propose a novel method that take all the frames into account together, inspired by the principles of bundle adjustment [26]. In order to maximize the utilization of information from all frames, we introduce a novel metric termed view consensus rate to assess the relationship between two masks, diverging from reliance on geometric overlap or semantic similarity. The key insight of the view consensus is that two 2D masks, whether from the same or different frames, should be considered as belonging to the same instance if a considerable number of other 2D masks from other views contain both these two masks. This view consensus leverages the good properties of modern 2D segmentation methods [30] that generates entity-level complete instance mask. Consequently, the same-instance relationship of two masks is robustly supported by multi-view observation, setting it apart from local measures of geometric or semantic similarity.

To further leverage all the frames, we construct a global mask graph where every node is a mask, and two view-consensus masks get connected. With this graph, we iteratively merges the candidate mask pairs to form clusters, achieving a globally consistent zero-shot 3D segmentation. Specifically, mask pairs with solid view consensus will be priority merged to a mask cluster, and then the view consensus of the mask cluster with other masks will be updated subsequently. During the clustering, the corresponding open-vocabulary features of masks within each cluster are also aggregated for open-vocabulary queries.

Through extensive experiments on publicly available datasets, MatterPort3D [1] and ScanNet200 [33]. Our method achieves SOTA performance on both open-vocabulary instance understanding and zero-shot 3D instance segmentation. We find our method significantly outperforms existing methods for segmenting fine-grained objects. *The code will be released to benefit the community.*

In summary, our contributions can be concluded as follows:

- A novel graph clustering based methodology to merge 2D

masks for 3D open-vocabulary instance segmentation.

- A novel view consensus metric for evaluating the relationship between masks, effectively leveraging global information from input image sequences.
- A SOTA open-vocabulary 3D instance segmentation method, which demonstrates superior performance on many publicly available datasets.

2. Related Works

Closed-set 3D instance segmentation. Since the emergence of 3D scene datasets [4, 9], the computer vision community has witnessed a large literature of 3D segmentation methods [3, 8, 11, 12, 14, 24, 32, 34, 38, 39]. These methods tackle this problem either in online [15, 25, 28, 44, 46] or offline [32, 34, 38, 39] manner, representing the scene as points cloud, voxels, and more recently neural field [37, 47]. Though significant progress has been made, these methods are limited to a closed-set category list which is predefined in certain dataset, suffering poor performance in open-vocabulary settings as tail classes that have few or no training examples. In contrast, our method aims to tackle open-vocabulary 3D instance segmentation that segment objects of arbitrary category.

Open-vocabulary 2D instance segmentation. The recent advances in large visual foundation models [2, 6, 22, 23, 30, 31] have enabled a remarkable level of robustness of 2D understanding tasks. Typical tasks include zero-shot 2D segmentation [2, 22, 30], open-vocabulary 2D image understanding [6, 23, 31], and open-vocabulary 2D object detection [19, 21, 48]. Recently, many works [9, 18, 36, 40, 41] focus on the open-vocabulary 2D segmentation task, which requires predicting the open-vocabulary feature at the pixel level. These methods encode 2D images and align open-vocabulary pixel features with them. However, due to the lack of large-scale 3D annotated data, end-to-end open-vocabulary 3D instance segmentation is in slow progress. In this work, we tackle the open-vocabulary 3D instance segmentation by leveraging the prior from large 2D vision-language models.

Open-vocabulary 3D instance segmentation. There are two types of methods: (1) 2D-to-3D region grow-based methods and (2) 3D-to-2D projection methods. (1) 2D-to-3D region grow-based methods [7, 27] propose to online fuse 2D observation to 3D instance segmentation. These methods represent the 3D instance in point clouds [27] and node graph [7]. By back-projecting the 2D mask to 3D point cloud, these methods leverage clustering algorithm [5] or geometry overlapping to find corresponding 3D instances. The open-vocabulary feature is also aggregated during the back-projection. However, these types of methods consider the associations between historical constructed 3D instances with live frame, lacking a global understanding of all observed frames. (2) 2D-to-2D projec-

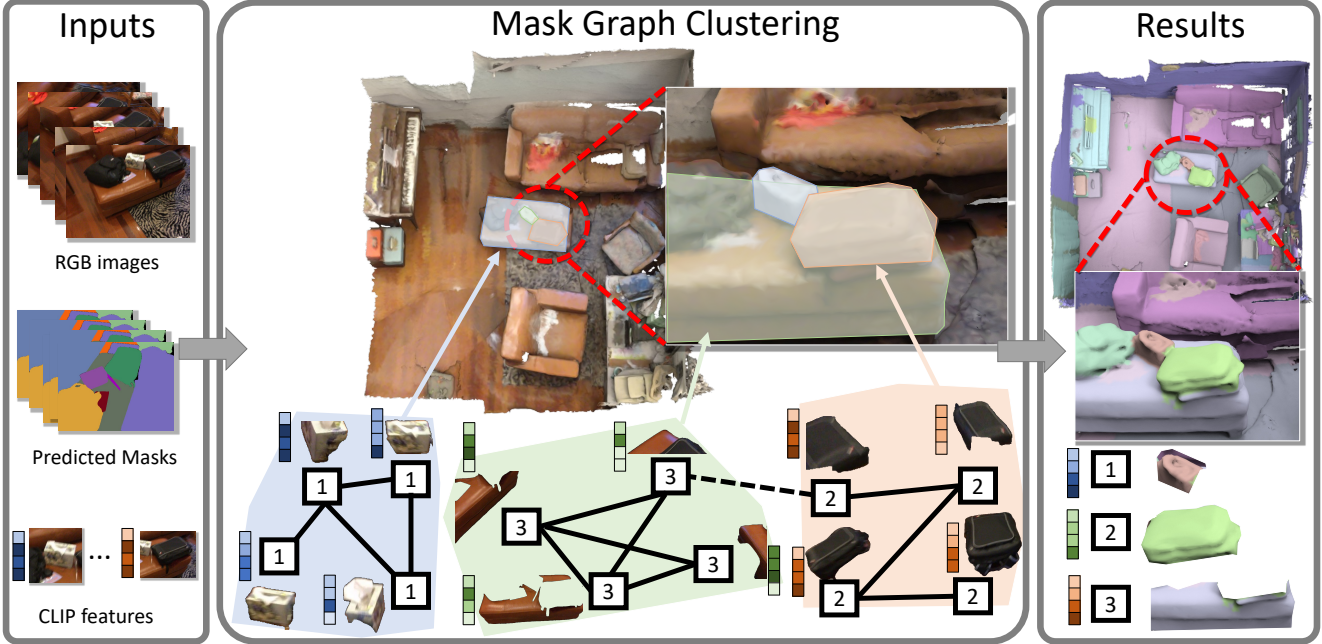


Figure 2. **Method overview.** (Left) Our method takes RGB images as inputs and obtains the corresponding instance segmentation and open-vocabulary feature from CropFormer [30] and CLIP [31]. (Middle) The masks serve as nodes in the mask graph, with connected edges filtered through view consensus. Subsequently, mask clustering is applied to identify clusters with high view consensus. (Right) These mask clusters are then back-projected to derive 3D instances, and corresponding CLIP features are aggregated for open-vocabulary queries.

tion methods [17, 29, 35] directly conduct 3D instance segmentation [17, 34] on 3D indoor scene input. They project the 3D instance objects to 2D frames, and extract open-vocabulary features for final aggregation. However, these types of methods are limited to well-reconstructed scene and detailed objects are easily missed if the geometry details are poor.

3. Method

3.1. Problem Formulation and Method Overview

Given a set of posed color images $\{I_1^c, I_2^c, \dots, I_T^c\}$, their corresponding depths $\{I_1^d, I_2^d, \dots, I_T^d\}$, and the reconstructed point cloud P of a scene, our algorithm outputs a list of 3D instances along with their open-vocabulary semantics fused from 2D mask proposals.

We initially employ an off-the-shelf, class-agnostic mask predictor to process each color image I_t^c and derive the 2D masks $\{m_{t,i} \mid i = 1, 2, \dots, n_t\}$. We assume the mask predictor to generate entity-level panoptic segmentation masks, indicating that each mask approximates one object with nearly all pixels assigned to a single mask. This assumption aligns with capabilities of advanced segmentation tools like CropFormer[30].

The overview pipeline of our method is illustrated in Fig. 2. To fuse these 2D masks from different frames

into 3D instances, we propose to construct a mask graph $G = (V, E)$. Each node in V corresponds to a mask $m_{t,i}$, and an edge in E indicates that two masks are part of the same instance and should be merged. To assess edge connectivity, we propose to leverage consensus cues from multi-view observations and therefore introduce view consensus rate as a criterion (Sec. 3.2).

Once the mask graph is established, we initiate an iterative process to cluster masks and update edges, with a priority on merging mask pairs displaying solid view consensus (Sec. 3.3). The result of this iterative process is a list of clusters, each denoting a 3D instance and containing multiple masks. Within such a cluster, we aggregate the corresponding partial point clouds from the individual masks to form the ultimate 3D instance. Building on these correspondences between 2D masks and 3D instances, we perform feature fusion for a more comprehensive representation, which aids in open-vocabulary semantic prediction (Sec. 3.4).

3.2. Mask Graph Construction

In this subsection, we introduce view consensus rate, which serves as the criterion to determine edge connectivity between two masks (Sec.3.2.1). We then propose an efficient method for calculating this rate (Sec.3.2.2) and leverage this rate to filter out under-segmented masks

(Sec.3.2.3).

Notations and Definitions Given the reconstructed point cloud P and frame index t , for a mask $m_{t,i}$, we can obtain the mask point cloud $P_{t,i}$ by projecting onto P the backprojected point cloud of $m_{t,i}$ from I_t^d . Then we define the frame point cloud P_t as the union of all $P_{t,i}$ s for $i = 1, 2, \dots, n_t$, yielding $P_{t,i} \subset P_t \subset P$. We define a point p to be visible at frame t if $p \in P_t$. We then define a mask $m_{t',i}$ to be visible at frame t if at least $\tau_{vis} = 0.3$ of its total points from $P_{t',i}$ are visible and denote the visible part as $P_{t',i}^t$. We denote the set of frames where $m_{t',i}$ is visible as $F(m_{t',i})$. Finally, we define the approximate containment relationship of one point clouds P_i by another point cloud P_j as $P_i \sqsubset P_j$, if at least $\tau_{contain} = 0.8$ of the total points in P_i lie within P_j .

3.2.1 View Consensus Rate

The cornerstone of our method lies in determining whether two masks belong to the same instance. In this context, we propose to leverage view consensus cues, as detailed below.

To assess the relationship between two masks, specifically $m_{t',i}$ and $m_{t'',j}$, where t' and t'' may be the same or different frames, we utilize the masks $\{m_{t,k}\}$ from relevant views. The goal is to check if there is substantial consensus among the views supporting that these two masks represent the same 3D instance.

To be more specific, we first find all the frames O in which both of the two masks are visible, serving as the observers to the two masks, i.e., $O(m_{t',i}, m_{t'',j}) = F(m_{t',i}) \cap F(m_{t'',j})$. And we denote the number of observers in O as $n(m_{t',i}, m_{t'',j}) = |O(m_{t',i}, m_{t'',j})|$, where $|\cdot|$ represents the cardinality of the set.

We then check whether an observer frame $t \in O$ supports the merging of these two masks. For an observer frame $t \in O$, if there exists a mask $m_{t,k}$ whose corresponding point cloud $P_{t,k}$ approximately contains both the point clouds $P_{t',i}^t$ of $m_{t',i}$ and $P_{t'',j}^t$ of $m_{t'',j}$, i.e., $P_{t',i}^t \sqsubset P_{t,k}$ and $P_{t'',j}^t \sqsubset P_{t,k}$, then this observer supports that the two masks are components of the same instance. The total number of supporters would be $n_{supporter}(m_{t',i}, m_{t'',j}) = |\{t \in O(m_{t',i}, m_{t'',j}) \mid \exists k, s.t. P_{t',i}^t, P_{t'',j}^t \sqsubset P_{t,k}\}|$. The proportion of supporters among all observers is subsequently defined as the **view consensus rate** c , as illustrated below:

$$c(m_{t',i}, m_{t'',j}) = \frac{n_{supporter}(m_{t',i}, m_{t'',j})}{n(m_{t',i}, m_{t'',j})} \quad (1)$$

An illustration of this view consensus rate can be found in Fig. 3.

Employing the consensus rate as a criterion, we connect edges between mask pairs whose view consensus rates exceeding a predefined threshold $\tau_{rate} = 0.9$. This procedure

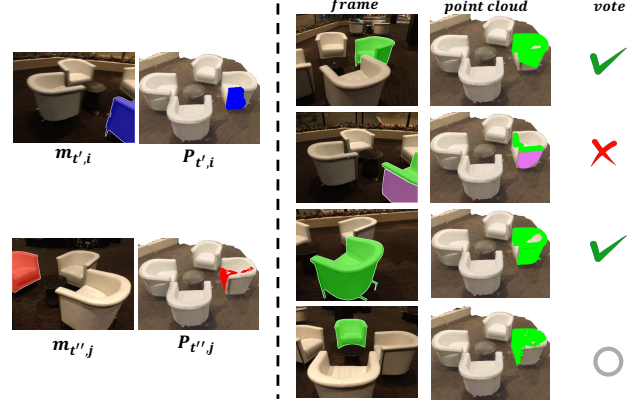


Figure 3. **View consensus rate.** Masks $m_{t',i}$ and $m_{t'',j}$ (side and frontal view of an armchair) are both visible in three frames, with two supporting them belonging to the same instance, resulting in a 2/3 consensus rate. Each mask is accompanied by its respective mask point cloud, displayed on the right. All point clouds are rendered under a consistent camera pose for clarity.

yields the set of edges E as follows:

$$E = \{\{m_{t',i}, m_{t'',j}\} \mid c(m_{t',i}, m_{t'',j}) \geq \tau_{rate}\} \quad (2)$$

Leveraging predictions across the entire sequence of images, our criterion shows enhanced robustness against over-segmentation errors compared to approaches that solely depend on local geometric overlap. Illustrated in Fig. 3, the two masks exhibit low geometric overlap despite belonging to the same armchair. However, our approach identifies a high consensus rate for them. This is attributed to the outstanding overall performance of modern mask predictors, which consistently segment this armchair comprehensively in most frames, encompassing both parts and thus yielding a high view consensus rate.

3.2.2 Efficient Computation of View Consensus Rate

Naively computing view consensus rates for all mask pairs can be untractable with a time complexity of $\mathcal{O}(N^2T)$, where N represents the total number of masks, i.e., $N = \sum_t n_t$. To speed up, we initially calculate and store the intermediate result to eliminate redundant computations.

Specifically, for each mask $m_{t',i}$, we first find $F(m_{t',i})$ and then identify all the masks that approximately contain it, denoted as $M(m_{t',i}) = \{m_{t,k} \mid t \in F(m_{t',i}) \text{ and } P_{t',i}^t \sqsubset P_{t,k}\}$. With these intermediate results, the computation of equation 1 can be simplified as,

$$c(m_{t',i}, m_{t'',j}) = \frac{|M(m_{t',i}) \cap M(m_{t'',j})|}{|F(m_{t',i}) \cap F(m_{t'',j})|} \quad (3)$$

In this way, all the operations in this expression have been simplified to simple set intersection operations involving

only a few dozen elements, leading to a significant reduction in computational complexity.

We now introduce the efficient computation of $M(m_{t',i})$. Initially, we examine the mask ID distribution of $P_{t',i}^t$ at frame t . If this distribution is concentrated, with more than $\tau_{contain} = 0.8$ of elements equalling k , it indicates that $P_{t',i}^t$ primarily constitutes a part of the k -th instance at frame t . By definition, $P_{t',i}^t \sqsubset P_{t,k}$. The mask ID distribution is denoted as $d(m_{t',i}, t)$, and we elaborate on its efficient calculation through a space-time trade-off in the implementation details (Sec. 3.5).

3.2.3 Under-Segment Mask Filtering

We can also identify whether a mask is under-segmented based on the mask ID distribution $d(m_{t',i}, t)$. If $d(m_{t',i}, t)$ exhibits a very diverse distribution, it signifies that $P_{t',i}$ comprises multiple instances at frame t , making it highly likely that $m_{t',i}$ is an under-segmented mask. Assuming most 2D mask predictor outputs are correct, we ignore the alternative explanation that $m_{t',i}$ is accurate but the mask predictor over-segments this object consistently in other views.

Therefore, under-segmentation is marked by frequent distinction of $P_{t',i}$ into parts. We track the frequency of such occurrences (number of frames with diverse distributions in $d(m_{t',i}, t) / |F(m_{t',i})|$). If this frequency exceeds $\tau_{filter} = 0.2$, we classify the mask as under-segmented and filter it out. Specifically, we remove it from the mask graph. Additionally, to prevent this mask from erroneously inflating the consensus rate between two masks belonging to different instances, we also eliminate it from all $M(m_{t',j})$ and remove t' from $F(m_{t',j})$.

3.3. Iterative Graph Clustering

Building upon the mask graph, we introduce an iterative graph clustering technique to merge masks and update the graph structure alternately. In the last iteration, each cluster denotes an instance.

When determining which masks to merge, we consider two strategies: 1) merging each maximal clique (where a clique is a subset of the graph with an edge between every pair of nodes); 2) merging each connected component (where a connected component is a subset of the graph with a path between every pair of nodes). The first approach, though precise, tends to be overly stringent, often leading to insufficient merging and excessive over-segmentation. The second approach, more permissive, relies on the correctness of every pair-wise identified same-instance relationship, which can be less reliable when the number of observers n —the denominator of c —is low.

To balance these strategies, we modify the second approach to prioritize merging masks with a high number of

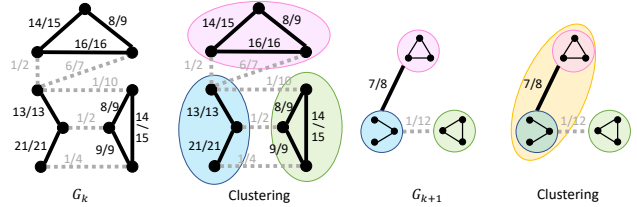


Figure 4. Illustration of iterative clustering. Node pairs with more observers are prioritized clustered (G_k). Then, view consensus of grouped masks is updated for the next clustering with more confident view consensus measurements. The text on the edge means $n_{support}/n$.

observers first, postponing less reliable connections to later iterations.

As illustrated in Fig. 4, in each iteration k , we set an observer threshold n_k and edges with $n < n_k$ are disconnected. We then identify connected components in the graph and merge them into new nodes. For a newly formed mask m_{new} from a set of masks $\{m_{t_1,i_1}, m_{t_2,i_2}, \dots, m_{t_s,i_s}\}$, its point cloud P_{new} is the union of $\{P_{t_1,i_1}, P_{t_2,i_2}, \dots, P_{t_s,i_s}\}$.

Subsequent to these node merging operations, updating edges requires recalculating the view consensus rate for the new mask in relation to others. Referring to equation 3, we calculate $F(m_{new})$ and $M(m_{new})$. While these two sets can be computed using the same technique as introduced in Sec. 3.2.2, we propose a method to accelerate this calculation while achieving comparable results through a straightforward approximation. Specifically, we approximate $F(m_{new})$ as $F(m_{t_1,i_1}) \cup F(m_{t_2,i_2}) \dots \cup F(m_{t_s,i_s})$ and $M(m_{new})$ as $M(m_{t_1,i_1}) \cup M(m_{t_2,i_2}) \dots \cup M(m_{t_s,i_s})$. This approximation is justified since masks merged due to high consensus rates often share containment by the same mask in frames where they both appear.

After each iteration k , a new graph G_{k+1} is formed. The observer threshold n_k is adjusted downwards over several iterations to avoid neglecting smaller objects visible in fewer frames. We adopt a decreasing n_k schedule, ranging from the top 5%, 10%, to 95% of observer counts across all mask pairs.

3.4. Open-Vocabulary Feature Aggregation

After multiple iterations of clustering, we have obtained a conclusive list where each entry represents a 3D instance proposal. Simultaneously, we maintain a corresponding list of masks associated with each instance. This 2D-3D relationship allows us to directly select representative masks and fuse their semantic features to create an open-vocabulary feature for this instance. Following OpenMask3D[35], we first pick the top-5 masks that best cover the instance. Subsequently, we crop the original RGB image at multiple scales around each mask and input these

Table 1. **Semantic 3D instance segmentation results on ScanNet200.** We report three average precision metrics, overall AP, AP with 25% and 50% IoU threshold, on all categories and three subsets. Mask3D and OpenMask3D both require supervised (sup.) training on ScanNet200. In fully zero shot (z.s.) setting, our method surpass OVIR-3D by a large margin on all metrics.

Model	Overall			Head			Common			Tail		
	AP	AP_{50}	AP_{25}									
<i>sup. mask + sup. semantic</i>												
Mask3D	26.9	36.2	41.4	39.9	54.3	61.3	21.7	29.6	34.2	17.9	22.8	26.4
<i>sup. mask + z.s. semantic</i>												
OpenMask3D	15.1	19.6	22.6	15.8	20.0	22.8	13.9	17.4	20.0	15.9	21.6	25.7
<i>z.s. mask + z.s. semantic</i>												
OVIR-3D	9.3	18.7	25.0	9.8	17.7	24.3	9.4	19.1	24.5	8.5	19.5	26.6
Ours	12.0	23.3	30.1	11.8	21.4	29.2	11.2	21.9	28.1	13.3	27.1	33.5

image crops into CLIP[31] to extract open-vocabulary features. The final instance feature is derived from the average pooling result of these features.

3.5. Implementation Details

In order to obtain object-level masks, we use CropFormer [30] as our 2D mask predictor. For open-vocabulary feature extraction, we use CLIP[31] ViT-H. To get mask point cloud $P_{t,i}$, we first back-project each mask to get the raw point cloud and then ball query the reconstructed point cloud with radius = 2cm for ScanNet and 3cm for Matterport. We adopt the post-processing approach from OVIR-3D[27] to refine the output 3D instances by using DBSCAN algorithm to separate disconnected point clusters into distinct instances.

4. Experiments

In this section, we extensively evaluate our proposed method by comparing it with the previous state-of-the-art methods on publicly available 3D instance segmentation benchmarks. The experimental setup is detailed in Sec. 4.1. In Sec. 4.2 and 4.3, we comprehensively analysis statistics of semantic and class-agnostic 3D instance segmentation. The validation of all the components of our method is presented in Section 4.4.

4.1. Experimental Setup

Dataset ScanNet [4] is a popular benchmark for 3D instance segmentation. The recently updated version ScanNet200 [33] of this benchmark includes 200 categories, covering a wide range of classes. We use the validation set that contains 312 scenes. MatterPort3D [1] serves as a more demanding benchmark due to its building-level scenes. Notably, the view points of RGB-D images in MatterPort3D are significantly more sparse, with only at least ~600 frames for an entire house compared to the ~3000 frames typically found in a room from ScanNet. This sparsity intensifies the challenge of view association.

Baselines We select the recent SOTA methods on both supervised closed-set 3D instance segmentation and open-

vocabulary 3D instance segmentation. Mask3D [34] stands out as a state-of-the-art method which requires supervised training on ScanNet200. OpenMask3D [35] leverages supervised mask proposals from Mask3D and employs CLIP for open-vocabulary semantics aggregation. Different from our setting, both of them rely on supervised mask. OVIR-3D [27] utilize both zero-shot masks and semantics, merging zero-shot 2D masks with large geometric and semantic overlap and using K-Means to choose the most representative features from the per-frame semantic feature.

Metrics For 3D instance segmentation tasks, we leverage average precision (AP) which is widely applied in this field. We also provide more detailed metrics AP_{25} and AP_{50} that is the average precision with Intersection-over-Union (IoU) threshold at 25% and 50% respectively. To thoroughly assess the zero-shot 3D mask generation ability, we also present the class-agnostic AP, disregarding the accuracy of semantic labels in the evaluation.

4.2. Semantic 3D Instance Segmentation

ScanNet200. For all the categories in ScanNet200, we report the AP , AP_{50} , AP_{25} metric in the first 3 columns of Tabel. 1. Our method significantly outperforms fully zero-shot method, OVIR-3D, by +2.7 AP, +4.6 AP_{50} and +5.1 AP_{25} , which validates our deliberate globally optimal association design. Notably, we observe a substantial drop in our model’s metric from 30.1 AP_{25} to 12.0 AP on ScanNet200, which we attribute to ground truth granularity. Our model excels in segmenting small objects like items on counters, boxes on shelves, whereas the ground truth often treats them as a single object. Consequently, for objects containing smaller ones, the overlap between our predictions and ground truth may not be sufficiently high. This phenomenon is further illustrated in Figure 5.

The ScanNet200 categories are further divided into three subsets—head, common, and tail—according to their frequency in the training set. We conduct additional experiments on these subsets to assess the performance of all methods in the context of the long-tail distribution. It can be seen that Mask3D excels on *Head* but drops severely on

Table 2. **Semantic 3D instance segmentation results on MatterPort3D.**

Model	MatterPort3D		
	AP	AP_{50}	AP_{25}
Mask3D	2.5	4.5	6.7
OpenMask3D	4.6	8.5	13.0
OVIR-3D	6.3	16.4	24.4
Ours	9.2	19.7	26.5

Common and Tail, where less frequent training instances affect its performance. In contrast, the rest three methods that constitutes of at least one zero-shot component show consistent results, demonstrating a better generalizability.

MatterPort3D To further evaluate the generalizability, we directly test all algorithms on MatterPort3D test set in a zero-shot manner. To ensure a fair comparison, we exclude scenes that cause baselines to run out of memory from the test set, the remaining list is attached in the supplementary material. As demonstrated in Table 2, our method significantly outperforms all baselines. Furthermore, the fully zero-shot method OVIR-3D and ours exhibit similar performance on both ScanNet and MatterPort3D benchmarks. In contrast, methods utilizing modules trained on ScanNet experience a substantial decline in all metrics on MatterPort3D. This reinforces the importance of further exploring associating zero-shot 2D masks into 3D instances.

4.3. Class-Agnostic 3D Mask Generation

To assess the effectiveness of our proposed zero-shot mask generation module, we present class-agnostic AP on both datasets. Since OpenMask3D shares the same mask proposal module as Mask3D, we report the metric only for the remaining three methods.

Quantitative Comparison. Similar to the semantic instance segmentation setting, we observe a consistent pattern. As depicted in Table 3, the supervised method Mask3D excels on its training dataset, ScanNet200, but experiences a significant drop on MatterPort3D, underscoring the limited generalizability of current fully-supervised 3D models. In contrast, our method demonstrates superior performance on both datasets within the zero-shot setting.

Table 3. **Class-agnostic 3D mask generation results on ScanNet200 and MatterPort3D.** Numbers highlighted in gray indicate supervised learning results, while those highlighted in black represent zero-shot inference results.

Model	ScanNet200			MatterPort3D		
	AP	AP_{50}	AP_{25}	AP	AP_{50}	AP_{25}
Mask3D	39.7	53.6	62.5	4.4	9.8	20.6
OVIR-3D	14.4	27.5	38.8	5.9	13.9	24.6
Ours	17.4	33.3	46.7	8.3	18.9	33.4

Qualitative Comparison. In Fig. 5, we further show the visual results of our model. Our method shows excellent ability to segment small objects, *e.g.*, items on the counter in ScanNet a), boxes on the shelf in ScanNet b). These small objects are simply labeled as part of its containers in the ground truth, which cause the AP at higher IoU threshold of our method drops severely.

Compared to OVIR-3D, our method has three main advantages: i) OVIR-3D tends to over-segment large objects, such as the coffee table and the sofa chair in ScanNet (b), the right rug in the MatterPort3D example. In the contrary, our method merges these objects well based on view consensus as explained in Sec. 3.2.1. ii) The strict filtering process in OVIR-3D falsely filter out many objects, *e.g.*, counter and pictures in ScanNet a) while our method only conservatively filter out under-segment masks. iii) Our method can segment the wall, floor well.

4.4. Ablation Studies

In Table 4, we analyze key components of our method on ScanNet200—under-segment mask filtering and iterative clustering. Starting with a baseline using view consensus ratio, we merge masks within connected components. This simple approach matches OVIR-3D baseline performance. Upon adding under-segment mask filtering and iterative clustering, performance steadily rises from 10.0 AP to 11.7 AP , reaching peak performance when both modules are combined.

Table 4. **Ablation study on under-segment mask filtering and iterative clustering.**

under. filtering	iter. clustering	AP	AP_{50}	AP_{25}
		10.0	19.1	24.2
✓		11.0	21.2	27.5
	✓	11.7	22.3	29.2
✓	✓	12.0	23.3	30.1

We conducted additional evaluations to assess the robustness of our algorithm to variations in hyperparameters. For the mask visibility threshold τ_{vis} ranging from 0.2 to 0.4, the under-segment mask filtering threshold τ_{filter} ranging from 0.2 to 0.4, the consensus rate threshold τ_{rate} ranging from 0.8 to 1 and the approximate containment threshold $\tau_{contain}$ ranging from 0.7 to 0.9, our method consistently demonstrates satisfying performance.

Table 5. **Ablation study on Hyperparameters.**

	AP	AP_{50}	AP_{25}
$\tau_{vis}(0.2 - 0.4)$	11.9 ± 0.06	23.2 ± 0.09	30.1 ± 0.07
$\tau_{filter}(0.2 - 0.4)$	11.9 ± 0.05	23.3 ± 0.19	30.0 ± 0.18
$\tau_{rate}(0.8 - 1)$	11.8 ± 0.20	22.7 ± 0.52	28.9 ± 0.83
$\tau_{contain}(0.7 - 0.9)$	11.9 ± 0.10	23.3 ± 0.22	30.3 ± 0.20

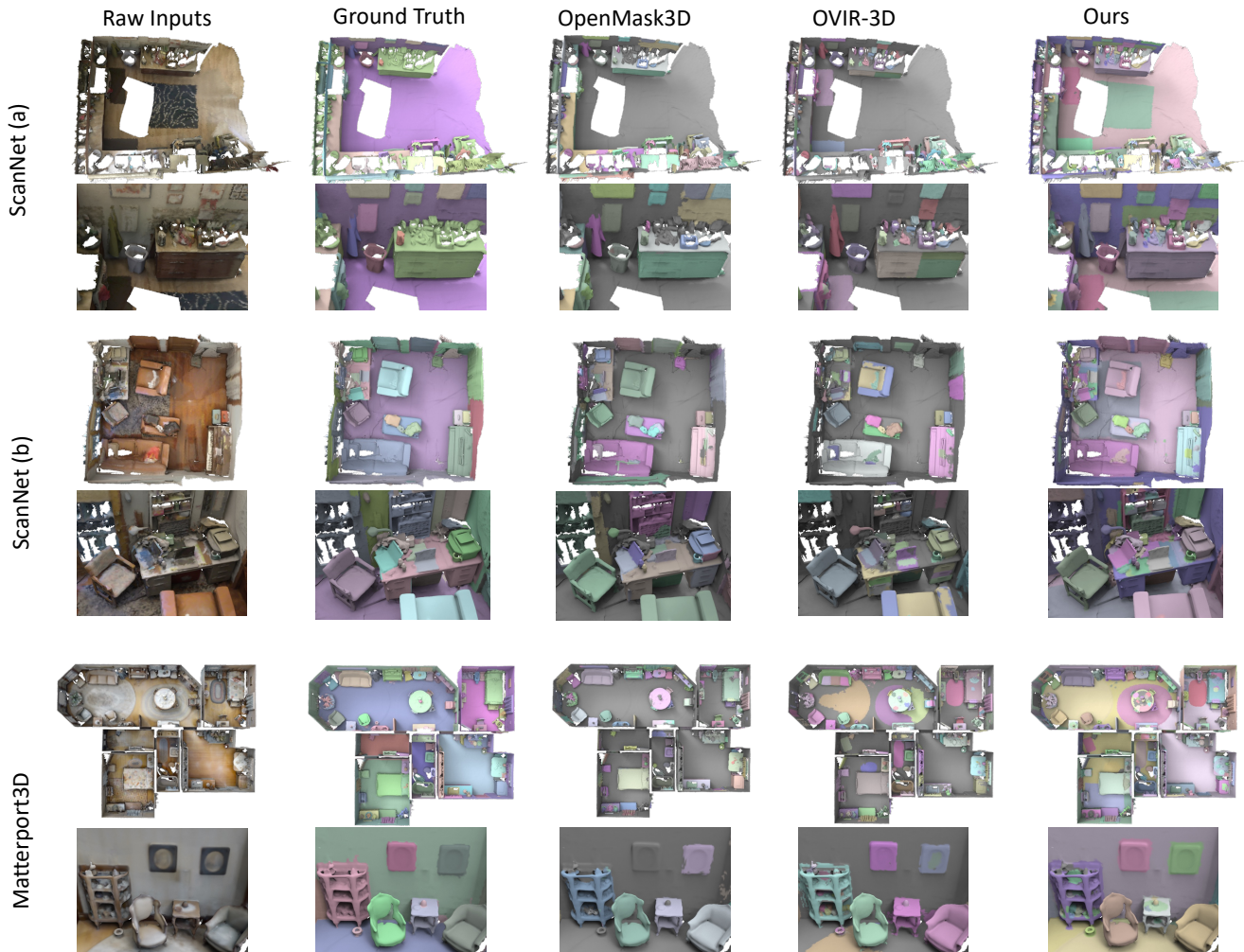


Figure 5. Comparison of 3D zero-shot segmentation performance. We compare our methods with OpenMask3D [35] and OVIR-3D [27] on ScanNet [4] and Matterport3D [1].

4.5. Limitations

Despite its impressive performance, there are two notable limitations: i) The accuracy of camera pose and depth map significantly influences our results. Instances of noisy camera pose or misaligned depth maps with RGB data can lead to significant overlap in our instance segmentation predictions. ii) The evaluation of open-vocabulary instance segmentation currently relies on closed-set benchmarks. These benchmarks often overlook small objects and may annotate them as part of nearby larger objects, such as clothes on a bed or items on a counter. Accurately evaluating methods in these cases remains a challenging task.

5. Conclusion

In this work, we propose a view consensus based mask graph clustering algorithm for open-vocabulary 3D in-

stance segmentation. Specifically, we present a novel view consensus metric to assess the relationship between masks, effectively utilizing global information from input image sequences. Using this metric, we construct a mask graph and iteratively cluster masks associated with the same 3D instances. During the clustering, corresponding open-vocabulary features of masks within each cluster are also aggregated for open-vocabulary queries. The results demonstrate that our method achieves SOTA performance on zero-shot instance segmentation and open-vocabulary instance understanding.

6. Acknowledgements

This work was supported in part by National Key R&D Program of China 2022ZD0160801.

References

- [1] Angel Chang, Angela Dai, Thomas Funkhouser, Maciej Halber, Matthias Niessner, Manolis Savva, Shuran Song, Andy Zeng, and Yinda Zhang. Matterport3d: Learning from rgb-d data in indoor environments. *arXiv preprint arXiv:1709.06158*, 2017. [2](#), [6](#), [8](#)
- [2] Bowen Cheng, Anwesa Choudhuri, Ishan Misra, Alexander Kirillov, Rohit Girdhar, and Alexander G Schwing. Mask2former for video instance segmentation. *arXiv preprint arXiv:2112.10764*, 2021. [2](#)
- [3] Christopher Choy, JunYoung Gwak, and Silvio Savarese. 4d spatio-temporal convnets: Minkowski convolutional neural networks. In *Proceedings of the IEEE/CVF conference on computer vision and pattern recognition*, pages 3075–3084, 2019. [2](#)
- [4] Angela Dai, Angel X Chang, Manolis Savva, Maciej Halber, Thomas Funkhouser, and Matthias Nießner. Scannet: Richly-annotated 3d reconstructions of indoor scenes. In *Proceedings of the IEEE conference on computer vision and pattern recognition*, pages 5828–5839, 2017. [1](#), [2](#), [6](#), [8](#)
- [5] Martin Ester, Hans-Peter Kriegel, Jörg Sander, Xiaowei Xu, et al. A density-based algorithm for discovering clusters in large spatial databases with noise. In *kdd*, pages 226–231, 1996. [2](#)
- [6] Golnaz Ghiasi, Xiuye Gu, Yin Cui, and Tsung-Yi Lin. Scaling open-vocabulary image segmentation with image-level labels. In *European Conference on Computer Vision*, 2021. [2](#)
- [7] Qiao Gu, Ali Kuwajerwala, Sacha Morin, Krishna Murthy Jatavallabhula, Bipasha Sen, Aditya Agarwal, Corban Rivera, William Paul, Kirsty Ellis, Ramalingam Chellappa, Chuang Gan, Celso Miguel de Melo, Joshua B. Tenenbaum, Antonio Torralba, Florian Shkurti, and Liam Paull. Conceptgraphs: Open-vocabulary 3d scene graphs for perception and planning. *ArXiv*, abs/2309.16650, 2023. [1](#), [2](#)
- [8] Lei Han, Tian Zheng, Lan Xu, and Lu Fang. Occuseg: Occupancy-aware 3d instance segmentation. In *Proceedings of the IEEE/CVF conference on computer vision and pattern recognition*, pages 2940–2949, 2020. [2](#)
- [9] Shuting He, Henghui Ding, and Wei Jiang. Semantic-promoted debiasing and background disambiguation for zero-shot instance segmentation. *2023 IEEE/CVF Conference on Computer Vision and Pattern Recognition (CVPR)*, pages 19498–19507, 2023. [1](#), [2](#)
- [10] Ji Hou, Angela Dai, and Matthias Nießner. 3d-sis: 3d semantic instance segmentation of rgb-d scans. In *Proceedings of the IEEE/CVF conference on computer vision and pattern recognition*, pages 4421–4430, 2019. [1](#)
- [11] Wenbo Hu, Hengshuang Zhao, Li Jiang, Jiaya Jia, and Tien-Tsin Wong. Bidirectional projection network for cross dimension scene understanding. In *Proceedings of the IEEE/CVF Conference on Computer Vision and Pattern Recognition*, pages 14373–14382, 2021. [2](#)
- [12] Zeyu Hu, Xuyang Bai, Jiayang Shang, Runze Zhang, Jiayu Dong, Xin Wang, Guangyuan Sun, Hongbo Fu, and Chiew-Lan Tai. Vmnet: Voxel-mesh network for geodesic-aware 3d semantic segmentation. In *Proceedings of the IEEE/CVF International Conference on Computer Vision*, pages 15488–15498, 2021. [2](#)
- [13] Chenguang Huang, Oier Mees, Andy Zeng, and Wolfram Burgard. Visual language maps for robot navigation. In *2023 IEEE International Conference on Robotics and Automation (ICRA)*, pages 10608–10615. IEEE, 2023. [1](#)
- [14] Jingwei Huang, Haotian Zhang, Li Yi, Thomas Funkhouser, Matthias Nießner, and Leonidas J Guibas. Texturenet: Consistent local parametrizations for learning from high-resolution signals on meshes. In *Proceedings of the IEEE/CVF Conference on Computer Vision and Pattern Recognition*, pages 4440–4449, 2019. [2](#)
- [15] Shi-Sheng Huang, Ze-Yu Ma, Tai-Jiang Mu, Hongbo Fu, and Shi-Min Hu. Supervoxel convolution for online 3d semantic segmentation. *ACM Transactions on Graphics (TOG)*, 40(3): 1–15, 2021. [2](#)
- [16] Zhening Huang, Xiaoyang Wu, Xi Chen, Hengshuang Zhao, Lei Zhu, and Joan Lasenby. Openins3d: Snap and lookup for 3d open-vocabulary instance segmentation. *ArXiv*, abs/2309.00616, 2023. [1](#), [2](#)
- [17] Zhening Huang, Xiaoyang Wu, Xi Chen, Hengshuang Zhao, Lei Zhu, and Joan Lasenby. Openins3d: Snap and lookup for 3d open-vocabulary instance segmentation. *arXiv preprint arXiv:2309.00616*, 2023. [2](#), [3](#)
- [18] Dat T. Huynh, Jason Kuen, Zhe nan Lin, Jiuxiang Gu, and Ehsan Elhamifar. Open-vocabulary instance segmentation via robust cross-modal pseudo-labeling. *2022 IEEE/CVF Conference on Computer Vision and Pattern Recognition (CVPR)*, pages 7010–7021, 2021. [1](#), [2](#)
- [19] Prannay Kaul, Weidi Xie, and Andrew Zisserman. Multimodal classifiers for open-vocabulary object detection. *arXiv preprint arXiv:2306.05493*, 2023. [2](#)
- [20] Justin Kerr, Chung Min Kim, Ken Goldberg, Angjoo Kanazawa, and Matthew Tancik. Lurf: Language embedded radiance fields. In *Proceedings of the IEEE/CVF International Conference on Computer Vision*, pages 19729–19739, 2023. [1](#)
- [21] Dahun Kim, Anelia Angelova, and Weicheng Kuo. Region-aware pretraining for open-vocabulary object detection with vision transformers. In *Proceedings of the IEEE/CVF Conference on Computer Vision and Pattern Recognition*, pages 11144–11154, 2023. [2](#)
- [22] Alexander Kirillov, Eric Mintun, Nikhila Ravi, Hanzi Mao, Chloe Rolland, Laura Gustafson, Tete Xiao, Spencer Whitehead, Alexander C Berg, Wan-Yen Lo, et al. Segment anything. *arXiv preprint arXiv:2304.02643*, 2023. [2](#)
- [23] Boyi Li, Kilian Q. Weinberger, Serge J. Belongie, Vladlen Koltun, and René Ranftl. Language-driven semantic segmentation. *ArXiv*, abs/2201.03546, 2022. [2](#)
- [24] Jinke Li, Xiao He, Yang Wen, Yuan Gao, Xiaoqiang Cheng, and Dan Zhang. Panoptic-phnet: Towards real-time and high-precision lidar panoptic segmentation via clustering pseudo heatmap. In *Proceedings of the IEEE/CVF Conference on Computer Vision and Pattern Recognition*, pages 11809–11818, 2022. [2](#)
- [25] Leyao Liu, Tian Zheng, Yun-Jou Lin, Kai Ni, and Lu Fang. Ins-conv: Incremental sparse convolution for online 3d segmentation. In *Proceedings of the IEEE/CVF Conference*

- on *Computer Vision and Pattern Recognition*, pages 18975–18984, 2022. [2](#)
- [26] Manolis IA Lourakis and Antonis A Argyros. Sba: A software package for generic sparse bundle adjustment. *ACM Transactions on Mathematical Software (TOMS)*, 36(1):1–30, 2009. [2](#)
- [27] Shiyang Lu, Haonan Chang, Eric Pu Jing, Abdeslam Boularias, and Kostas E. Bekris. Ovir-3d: Open-vocabulary 3d instance retrieval without training on 3d data. *ArXiv*, abs/2311.02873, 2023. [1](#), [2](#), [6](#), [8](#)
- [28] Gaku Narita, Takashi Seno, Tomoya Ishikawa, and Yohsuke Kaji. Panopticfusion: Online volumetric semantic mapping at the level of stuff and things. In *2019 IEEE/RSJ International Conference on Intelligent Robots and Systems (IROS)*, pages 4205–4212. IEEE, 2019. [2](#)
- [29] Songyou Peng, Kyle Genova, Chiyu Jiang, Andrea Tagliasacchi, Marc Pollefeys, Thomas Funkhouser, et al. Openscene: 3d scene understanding with open vocabularies. In *Proceedings of the IEEE/CVF Conference on Computer Vision and Pattern Recognition*, pages 815–824, 2023. [3](#)
- [30] Lu Qi, Jason Kuen, Tiancheng Shen, Jiuxiang Gu, Wenbo Li, Weidong Guo, Jiaya Jia, Zhe Lin, and Ming-Hsuan Yang. High quality entity segmentation. In *Proceedings of the IEEE/CVF International Conference on Computer Vision*, pages 4047–4056, 2023. [2](#), [3](#), [6](#)
- [31] Alec Radford, Jong Wook Kim, Chris Hallacy, Aditya Ramesh, Gabriel Goh, Sandhini Agarwal, Girish Sastry, Amanda Askell, Pamela Mishkin, Jack Clark, et al. Learning transferable visual models from natural language supervision. In *International conference on machine learning*, pages 8748–8763. PMLR, 2021. [2](#), [3](#), [6](#)
- [32] Damien Robert, Bruno Vallet, and Loic Landrieu. Learning multi-view aggregation in the wild for large-scale 3d semantic segmentation. In *Proceedings of the IEEE/CVF Conference on Computer Vision and Pattern Recognition*, pages 5575–5584, 2022. [2](#)
- [33] David Rozenberszki, Or Litany, and Angela Dai. Language-grounded indoor 3d semantic segmentation in the wild. In *European Conference on Computer Vision*, pages 125–141. Springer, 2022. [1](#), [2](#), [6](#)
- [34] Jonas Schult, Francis Engelmann, Alexander Hermans, Or Litany, Siyu Tang, and Bastian Leibe. Mask3d for 3d semantic instance segmentation. *arXiv preprint arXiv:2210.03105*, 2022. [2](#), [3](#), [6](#)
- [35] Ayça Takmaz, Elisabetta Fedele, Robert W Sumner, Marc Pollefeys, Federico Tombari, and Francis Engelmann. Openmask3d: Open-vocabulary 3d instance segmentation. *arXiv preprint arXiv:2306.13631*, 2023. [1](#), [3](#), [5](#), [6](#), [8](#)
- [36] VS Vibashan, Ning Yu, Chen Xing, Can Qin, Mingfei Gao, Juan Carlos Niebles, Vishal M. Patel, and Ran Xu. Mask-free ovis: Open-vocabulary instance segmentation without manual mask annotations. *2023 IEEE/CVF Conference on Computer Vision and Pattern Recognition (CVPR)*, pages 23539–23549, 2023. [1](#), [2](#)
- [37] Suhani Vora, Noha Radwan, Klaus Greff, Henning Meyer, Kyle Genova, Mehdi SM Sajjadi, Etienne Pot, Andrea Tagliasacchi, and Daniel Duckworth. Nesf: Neural semantic fields for generalizable semantic segmentation of 3d scenes. *arXiv preprint arXiv:2111.13260*, 2021. [2](#)
- [38] Thang Vu, Kookhoi Kim, Tung M Luu, Thanh Nguyen, Junyeong Kim, and Chang D Yoo. Softgroup++: Scalable 3d instance segmentation with octree pyramid grouping. *arXiv preprint arXiv:2209.08263*, 2022. [2](#)
- [39] Thang Vu, Kookhoi Kim, Tung M Luu, Thanh Nguyen, and Chang D Yoo. Softgroup for 3d instance segmentation on point clouds. In *Proceedings of the IEEE/CVF Conference on Computer Vision and Pattern Recognition*, pages 2708–2717, 2022. [2](#)
- [40] Haoxiang Wang, Pavan Kumar Anasosalu Vasu, Fartash Faghri, Raviteja Vemulapalli, Mehrdad Farajtabar, Sachin Mehta, Mohammad Rastegari, Oncel Tuzel, and Hadi Pouransari. Sam-clip: Merging vision foundation models towards semantic and spatial understanding. *ArXiv*, abs/2310.15308, 2023. [1](#), [2](#)
- [41] Jianzong Wu, Xiangtai Li, Henghui Ding, Xia Li, Guangliang Cheng, Yu Tong, and Chen Change Loy. Betrayed by captions: Joint caption grounding and generation for open vocabulary instance segmentation. *ArXiv*, abs/2301.00805, 2023. [1](#), [2](#)
- [42] Kashu Yamazaki, Taisei Hanyu, Khoa Vo, Thang Pham, Minh Tran, Gianfranco Doretto, Anh Nguyen, and Ngan Le. Open-fusion: Real-time open-vocabulary 3d mapping and queryable scene representation. *arXiv preprint arXiv:2310.03923*, 2023. [1](#)
- [43] Yunhan Yang, Xiaoyang Wu, Tong He, Hengshuang Zhao, and Xihui Liu. Sam3d: Segment anything in 3d scenes. *arXiv preprint arXiv:2306.03908*, 2023. [1](#)
- [44] Jiazhao Zhang, Chenyang Zhu, Lintao Zheng, and Kai Xu. Fusion-aware point convolution for online semantic 3d scene segmentation. In *Proceedings of the IEEE/CVF conference on computer vision and pattern recognition*, pages 4534–4543, 2020. [2](#)
- [45] Jiazhao Zhang, Liu Dai, Fanpeng Meng, Qingnan Fan, Xuelin Chen, Kai Xu, and He Wang. 3d-aware object goal navigation via simultaneous exploration and identification. In *Proceedings of the IEEE/CVF Conference on Computer Vision and Pattern Recognition*, pages 6672–6682, 2023. [1](#)
- [46] Lintao Zheng, Chenyang Zhu, Jiazhao Zhang, Hang Zhao, Hui Huang, Matthias Niessner, and Kai Xu. Active scene understanding via online semantic reconstruction. In *Computer Graphics Forum*, pages 103–114. Wiley Online Library, 2019. [2](#)
- [47] Shuaifeng Zhi, Tristan Laidlow, Stefan Leutenegger, and Andrew J Davison. In-place scene labelling and understanding with implicit scene representation. In *Proceedings of the IEEE/CVF International Conference on Computer Vision*, pages 15838–15847, 2021. [2](#)
- [48] Xingyi Zhou, Rohit Girdhar, Armand Joulin, Philipp Krähenbühl, and Ishan Misra. Detecting twenty-thousand classes using image-level supervision. In *European Conference on Computer Vision*, pages 350–368. Springer, 2022. [2](#)